The Complex Structure of the Mg II $\lambda\lambda$ 2795.523, 2802.698 Å Regions of 64 Be Stars

Evaggelia Lyratzi,[1] Emmanouel Danezis,[1] Luka Č. Popović,[2]
Milan S. Dimitrijević,[2] Dimitris Nikolaidis,[1] and Antonis Antoniou[1]

[1]*University of Athens, Faculty of Physics, Department of Astrophysics, Astronomy and Mechanics,*
Panepistimioupoli, Zographou 157 84, Athens, Greece
[2]*Astronomical Observatory of Belgrade, Volgina 7, 11160 Belgrade, Serbia*
Isaac Newton Institute of Chile, Yugoslavia Branch
elyratzi@phys.uoa.gr, edanezis@phys.uoa.gr, lpopovic@aob.bg.ac.yu, mdimitrijevic@aob.bg.ac.yu, ananton@phys.uoa.gr

Abstract

Here we consider the presence of absorption components shifted to the violet or red side of the main spectral line (satellite or discrete absorption components, i.e., SACs or DACs) in the regions of the Mg II resonance lines in Be stars as well as their kinematical characteristics. Namely, our objective is to check whether there exists a common physical structure for the atmospheric regions creating SACs or DACs of the Mg II resonance lines. In order to do this, a statistical study of the Mg II $\lambda\lambda$ 2795.523, 2802.698 Å lines in the spectra of 64 Be stars of all spectral subtypes and luminosity classes was performed. We found that the atmospherical absorption regions where the Mg II resonance lines originated may be formed of several independent density layers of matter that rotate with different velocities. It was also attempted to separate SACs and DACs according to low or high radial velocity. The emission lines were detected only in the earliest and latest spectral subtypes.

Key words: stars: atmospheres — stars: early type — stars: emission-line, Be — stars: kinematics

1. Introduction

The Mg II resonance lines have a peculiar profile in the Be stellar spectra, which indicates a multicomponent nature of their origin region. Many researchers have observed the existence of absorption components shifted to the violet or red side of the main spectral line (Underhill 1970; Marlborough et al. 1978; Dachs 1980; Doazan 1982; Danezis 1983, 1987; Sahade et al. 1984; Sahade & Brandi 1985; Hutsemékers 1985; Danezis et al. 1991; Doazan et al. 1991; Laskarides et al. 1992; Cidale 1998; Lyratzi et al. 2003). These components — Discrete Absorption Components (DACs: Bates & Halliwell 1986) or Satellite Absorption Components (SACs: Danezis et al. 2003; Lyratzi & Danezis 2004) — probably originate in separated regions that have different rotational and radial velocities. Especially in the case of very narrow DACs and SACs, they cannot be photospheric; rather, they have a circumstellar or interstellar origin (Slettebak & Snow 1978). For example, Kondo, Morgan, and Modisette (1976) found that the shell absorption becomes stronger in intermediate to late B stars, and suggested that "it might be due to the rising temperature in the gaseous shell which converts Mg II to Mg III and to the weakening of the outward-driving mechanisms of the atmosphere". In any case, the whole feature of the Mg II resonance lines is not the result of a uniform atmospherical region, but the components are created in different regions, which rotate and move radially with different velocities. As de Jager et al. (1979) proposed in their study of 33 stellar spectra of all the spectral types, variable mass loss in the late B supergiants occurs due to "occasional stellar 'puffs'

superposed on a more or less regular wind". They proposed that "there are concentrations of low-ionization species in the stellar wind as a result of the occurrence of significant density variations". Also, in order to explain the complex profiles of the Mg II resonance lines, Cidale (1998) proposed that the Be stellar atmospheres are composed of a classical photosphere, an extending high-temperature chromosphere, and a cool envelope. There is a question about the contributions of different atmospherical layers, especially in the case of SAC and/or DAC phenomena, in constructing profiles of the Mg II resonance lines.

The aim of this work is to statistically investigate the presence of SACs and/or DACs in regions of Mg II resonance lines in Be stars and their kinematical characteristics. Also, we would like to search some conclusion about the limits of the rotational and radial velocities ($V_{\rm rot}$, $V_{\rm rad}$), as well as to check whether there exists a common physical structure for the atmospherical regions that create the SACs of the Mg II resonance lines in the spectra of all the Be stars. To do that, a statistical study of the UV Mg II resonance lines $\lambda\lambda$ 2795.523, 2802.698 Å in the spectra of 64 Be stars (all the spectral subtypes and luminosity classes) was performed. The study was based on a model proposed by Danezis et al. (2003) and Lyratzi and Danezis (2004).

We decided to study the Mg II resonance lines, because they are characteristic of the cool envelope in Be stellar atmospheres and very intense features in the spectra of Be stars and they mostly present a complex and peculiar structure. Besides, since they are resonance lines, they give us a possibility to test the validity of the proposed model. Because we have to
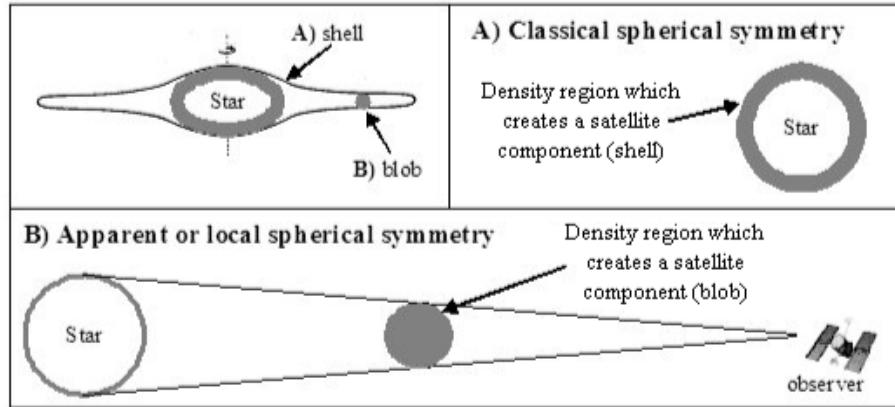
Fig. 1. Density regions that create the observed SACs or DACs in the stellar spectra.

adhere to all of the necessary physical criteria and techniques (Danezis et al. 2003). Our purpose here was to study spectral lines that are created in cool regions (Mg II) in Be stellar atmospheres. Danezis (1987), Sahade, Brandi, and Fontenla (1984), and Sahade and Brandi (1985) detected multistructures in the regions where Fe II lines (I.P.=7.870 eV) are created in the spectra of Be stars, which are characterized as iron stars. One of our purposes was to investigate whether the multistructure appears only in the Fe II spectral lines, or in also other spectral lines with a similar ionization potential (I.P.), as Mg II (I.P.=7.646 eV). This is another reason why we chose to study the Mg II resonance lines and not some other resonance lines of the cool envelope, as N II (I.P.=14.490 eV), C II (I.P.=11.260 eV), Si II (I.P.=8.110 eV), or Al II (I.P.=5.986 eV). The study of Mg II resonance lines provides us information not only about the cool envelope, but also about the multistructure of another ion that lies in the same region where the Fe II spectral lines are created.

In section 2, we describe the method of analysis, in section 3 the observational data, and in section 4 the results along with a discussion. In section 5 we give our conclusions.

2. Method of Spectral Line Analysis

Before describing the method used in our study, let us explain the differences between DACs and SACs. The DACs are components of a spectral line of a specific ion, shifted at different $\Delta\lambda$ from the transition wavelength of a line, because they are created in different density regions that rotate and move radially with different velocities (Lyratzi & Danezis 2004). The DACs are discrete lines, easily observed, in the spectra of some Be stars of luminosity class III, in the case of the Mg II doublet. However, if the layers that give rise to such lines rotate with quite large velocities and move radially with small velocities, then the produced lines are quite broadened and slightly shifted. As a result, they are blended among themselves as well as with the main spectral component, and thus they do not appear as being discrete; consequently, they cannot be resolved. In such a case, the name Discrete Absorption Component is inappropriate. Besides, as Peton (1974) first pointed out, these components appear as "satellites" in the violet or in the red side of the main spectral
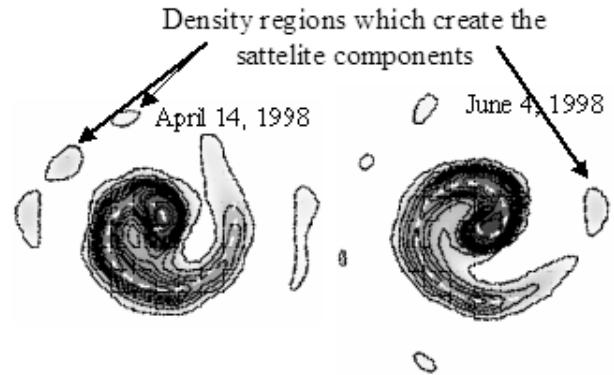
Fig. 2. Due to rotation of the star, the ejected matter forms spiral streams that produce blobs that create the observed SACs or DACs in the stellar spectra. This figure is taken from Tuthill, Monnier, and Danchi (1999).

line's component as a function of the time or the phase in the case of a binary system. For these two reasons, and in order to give a unique name to all of these lines that are components of the line profile whether they are discrete or not, it has been proposed (Lyratzi & Danezis 2004) that they should be named Satellite Absorption Components (SACs) as a general expression, because the Discrete Absorption Components (DACs) are "Satellites" of a main spectral line, while the SACs are not always discrete, and cannot be easily resolved.

An additional peculiar phenomenon is that all of the lines of a specific ion have not DACs. The DAC phenomenon is not a general one, but is present in the case of some lines that have a low excitation potential. For example, while the Mg II resonance lines at 2795.523, 2802.698 Å (multiplet 1) have DACs in the spectra of some Be stars, their subordinate lines at 2790.768, 2797.989 Å (multiplet 3) do not present the same phenomenon. Therefore, we decided to study the Mg II resonance lines, since they are the only Mg II doublet having DACs.

In order to obtain a qualitative picture, we will use the spherical geometry. According to it, there are two possibilities (see figure 1).

A) The region that creates the SACs or DACs may be an envelope around and near to a rapidly rotating star. In such a case, the spherical model could give only a rough approximation, but would allow us to obtain some qualitative results. We note that such an assumption is valid for some earlier models like, e.g., Doazan and Thomas (1982), which cannot explain the observed free-free emission or polarization, but we are interested here only in the kinematic characteristics. In this case, the calculated values of the radial velocity correspond to the component of the expansion or contraction velocity of the shell, which is projected to the observational axis.

B) The region which creates the SACs or DACs may be an independent density region (blob), which is spherically symmetric around its own center. Such density regions have been observed around stars that eject mass. In figure 2, we can see this phenomenon in WR 104, observed by Tuthill, Monnier, and Danchi (1999). Such a region may be one that creates the Mg II resonance lines, and that lies in a cool envelope of the stellar atmosphere. Such a blob may have three different motions: a) it may rotate around the star, b) it may expand or contract, and c) it may move radially. This means that the calculated values of the radial velocity consist of three different components: a) the component of the rotational velocity of the blob around the star, projected to the observational axis, b) the component of the expansion or contraction velocity of the blob, projected to the observational axis, and c) the component of the velocity of the blob's radial motion, projected to the line of sight.

In principle, as known, the star ejects mass with a specific radial velocity. The stream of matter is twisted, forming density regions, such as the interaction of fast and slow wind components, corotating interaction regions (CIRs), and structures due to magnetic fields or spiral streams as a result of the stellar rotation (Underhill & Fahey 1984; Mullan 1984a, 1984b, 1986; Prinja & Howarth 1988; Cranmer & Owocki 1996; Kaper et al. 1996, 1997, 1999; Fullerton et al. 1997; Cranmer et al. 2000). Consequently, hydrodynamic and magnetic forces act as centripetal forces, causing the outward moving matter to twist and move around the star (see figure 2). This motion of the matter is responsible for the formation of high-density regions (shells, blobs, puffs, and spiral streams), that are either spherically symmetric with respect to the star or with respect to their own center (Danezis et al. 2003; Lyratzi & Danezis 2004) (see figure 1).

In order to study the physical structure and the existence of SAC phenomena in the regions where these lines are created, we used a model proposed by Danezis et al. (2003) and Lyratzi and Danezis (2004). This model allowed us to calculate the rotational ($V_{\rm rot}$) and radial velocities ($V_{\rm rad}$) of independent density layers of matter in these regions, as well as the optical depth (τ) and the column density (n). If the considered SACs or DACs originate from "puffs" or "blobs" created by stellar winds in a cool extended envelope, the real shape of the envelope is not crucial. If the considered features are created in the envelope's layers, we could also reach some qualitative

conclusions, since we are interested only in the kinematical properties here. Moreover, because there is no sophisticated or rough model of a Be star that could fit the observed profiles, considering their complex structure, there are no results of similar investigations for comparison.

Let us consider that the area of gas that creates a specific spectral line consists of i independent absorbing density regions, followed by j independent regions that both absorb and emit and by an outer absorbing region. Such a structure produces DACs or SACs in the observed spectra (Danezis et al. 2003). The final line function which can describe the complex line profiles of the observed spectral lines is (Danezis et al. 2003; Lyratzi & Danezis 2004)

$$F_\lambda = [F_{\lambda 0} \prod_i e^{-L_i \xi_i} + \sum_j S_{\lambda {\rm e} j}(1 - e^{-L_{{\rm e}j}\xi_{{\rm e}j}})]e^{-L_g \xi_g} \quad (1)$$

where F_λ is the observed flux, $F_{\lambda 0}$ the initial flux, $S_{\lambda {\rm e} j}$ the source functions of each emitting density region, ξ the optical depth in the center of the line, and L_i, $L_{{\rm e}j}$, L_g the distribution functions of the absorption coefficients ($k_{\lambda i}$, $k_{\lambda {\rm e}j}$, $k_{\lambda g}$), respectively. Each L depends on the values of the rotational and the radial velocities of the density region, which forms each component of the spectral line ($V_{\rm rot}$, $V_{\rm rad}$) (Danezis et al. 2003; Lyratzi & Danezis 2004). The product of L and ξ is the optical depth of each region.

This function does not depend on the geometry of the regions creating the observed feature. The considered geometry of the regions is taken into account in order to define the distribution function, L. This means that L may represent any distribution which decides a certain geometry (see the Appendix), without changing anything in F_λ.

Each component of the spectral line, which is formed by the $i^{\rm th}$ density region of matter, must be accurately reproduced by the function $e^{-L_i \xi_i}$ by applying appropriate values of $V_{{\rm rot}_i}$, $V_{{\rm rad}_i}$ and ξ_i. Using the best model fit for a complex spectral line, we can calculate the apparent radial and rotational velocities ($V_{{\rm rad}_i}$, $V_{{\rm rot}_i}$) and the optical depth (ξ_i) in the center of the line of the region where the main spectral line and its SACs are created.

In the case where we want to consider that some other physical parameters are responsible for the line broadening, and not the rotation of the region that produces the studied spectral lines, we may replace the exponential $e^{-L\xi}$ with another classical distribution.

In the case of emission lines, each emission component, which is formed by the $j^{\rm th}$ density region of matter, must be accurately reproduced by the function $S_{\lambda {\rm e} j}(1 - e^{-L_{{\rm e}j}\xi_{{\rm e}j}})$, by applying the appropriate values of $V_{{\rm rot}_i}$, $V_{{\rm rad}_i}$, ξ_i, and S. Using the best model fit for a complex spectral line, we can calculate the apparent radial and rotational velocities ($V_{{\rm rad}_i}$, $V_{{\rm rot}_i}$), the optical depth (ξ_i) at the center of the line, and the source function, S, of the region where the emission component is created.

The proposed model is relatively simple, aiming to describe the regions where the spectral lines that present SACs are created. With this model we can study the regions of a specific ion that creates a specific spectral line.

This model presupposes that the main reason for the line broadening is rotation of the region that gives rise to the

Table 1. The list of Be stars.

Star	Spectral type	Camera	ref.	Star	Spectral type	Camera	ref.
HD 5394	B0 IV : evar	Lwr 07861	1	HD 25940	B3 V e	Lwr 05950	2
HD 53367*	B0 IV : e	Lwr 09286	1	HD 45725*	B3 V e	Lwp 10041	2
HD 203374†	B0 IV pe	Lwp 07400	1	HD 183362	B3 V e	Lwp 11044	2
HD 206773	B0 V : pe	Lwr 14808	1	HD 208057	B3 V e	Lwp 29221	2
HD 200310	B1 V e	Lwr 09544	1	HD 205637	B3 V : p	Lwr 05947	4
HD 212571	B1 V e	Lwr 05948	2	HD 217543	B3 V pe	Lwp 13326	2
HD 44458*	B1 V pe	Lwp 30173	1	HD 217050†	B4 III pe	Lwr 05933	2
HD 200120	B1.5 V nne	Lwr 11035	2	HD 89884	B5 III	Lwp 29529	6
HD 193237	B2 pe	Lwr 07990	2	HD 22192	B5 V e	Lwr 06898	2
HD 45910*	B2 III e	Lwr 12138	3	HD 23302	B6 III e	Lwr 09071	2
HD 37202	B2 IV p	Lwr 05888	4	HD 45542	B6 III e	Lwp 07631	2
HD 36576	B2 IV – V e	Lwp 14029	2	HD 109387	B6 III pe	Lwr 04132	2
HD 212076	B2 IV – V e	Lwr 03406	2	HD 23480	B6 IV e	Lwr 05219	2
HD 32991*	B2 V e	Lwr 11426	2	HD 217891	B6 V e	Lwr 09069	2
HD 58050	B2 V e	Lwr 14810	2	HD 138749	B6 V nne	Lwr 07858	2
HD 164284	B2 V e	Lwr 11038	2	HD 23630	B7 III	Lwr 09060	2
HD 41335	B2 V ne	Lwr 07384	2	HD 209409	B7 IV e	Lwp 15464	2
HD 52721	B2 V ne	Lwp 05462	5	HD 6811	B7 V e	Lwr 09070	7
HD 58343	B2 V ne	Lwr 07363	6	HD 192044*	B7 V e	Lwp 08135	8
HD 148184	B2 V ne	Lwr 06744	6	HD 210129	B7 V ne	Lwp 23173	7
HD 202904	B2 V e	Lwr 07343	2	HD 142983	B8 Ia/Iab	Lwr 07359	6
HD 65079	B2 V ne	Lwp 30119	5	HD 29866	B8 IV ne	Lwr 08745	2
HD 28497	B2 V ne	Lwr 07337	6	HD 47054	B8 V e	Lwp 13074	9
HD 45995*	B2 V nne	Lwr 08648	1	HD 183914*	B8 V e	Lwr 04609	9
HD 10516	B2 V pe	Lwr 07335	2	HD 50138	B8 V e	Lwr 09358	11
HD 187567*	B2.5 IV e	Lwp 14025	2	HD 58715	B8 V var	Lwp 10104	10
HD 191610	B2.5 V e	Lwr 07342	2	HD 23552†	B8 V ne	Lwr 08744	7
HD 32343*	B2.5 V e	Lwr 05890	2	HD 185037	B8 V ne	Lwp 08136	9
HD 65875	B2.5 V e	Lwr 05616	2	HD 199218	B8 V nne	Lwp 09903	7
HD 60855†	B2/B3 V	Lwp 15477	6	HD 91120	B8/B9 IV/V	Lwp 07475	6
HD 37490*	B3 III e	Lwr 07361	1	HD 142926	B9 pe	Lwr 05768	7
HD 50820	B3 IV e+...	Lwr 16776	2	HD 144	B9 III e	Lwr 08997	7

The list of Be stars with spectral type (columns 2, 6) and the type of the camera used during observations (columns 3, 7).

* Double system.

† Triple system.

References: (1) Morgan, Code, and Whitford (1955); (2) Lesh (1968); (3) Sahade, Brandi, and Fontenla (1984); (4) Herbig and Spalding (1955); (5) Guetter (1968); (6) Houk and Smith-Moore (1988); (7) Cowley (1972); (8) Osawa (1959); (9) Cowley et al. (1969); (10) Slettebak (1954); (11) Houziaux and Andrillat (1976).

spectral line (Doazan 1982). We can accept this assumption when we deal with the inner layers to the post coronal regions. Thus, for these atmospheric layers the model gives satisfactory results.

3. Observational Data and Fitting Procedure

The data that we used are the Mg II resonance lines of 64 Be stars taken from the International Ultraviolet Explorer (IUE) Archive Search database.[1] The stellar spectra were observed with the IUE satellite using the Long Wavelength range Prime and Redundant cameras (LWP, LWR) at high resolution (0.1 to 0.3 Å). In table 1, we give a list of stars, their spectral type, and the type of camera used during observations.

Our first step is to identify the spectral lines in the studied wavelength range, in order to determine which lines may be blended with the Mg II doublet, and thus may contribute to the observed features. The identification was made by using the NIST Atomic Spectra Database[2] as well as the catalogues of Moore (1968) and Kelly (1979). In this specific spectral range the adjacent features of the Mg II profiles are intense, but they are away from the Mg II spectral features, so that, in spite of their important influence on the wings, their much smaller influence in the central parts is not important for our discussion. Moreover, because we deal with resonance lines, we know that if one line of the doublet is well fitted, we should apply the same parameters to the other one, even if the fit is not very good. In this case, the unfitted regions correspond to blends.
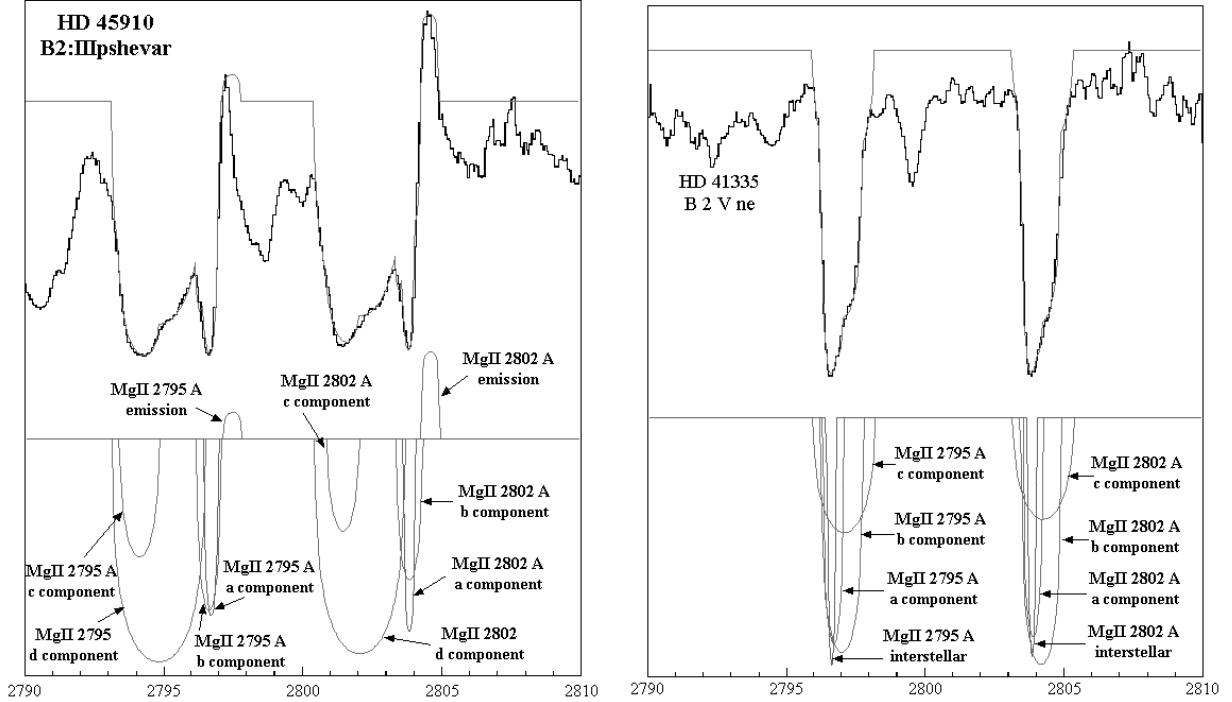
Fig. 3. Mg II resonance line profiles fitted with the model for HD 45910 and HD 41335. The thick lines present observations, and the thin lines present the best fit. The DACs (HD 45910) and SACs (HD 41335) are present below.

Also, the level of the continuum is calculated for the whole spectrum taken by IUE. This means that its suppression by the blends does not affect our calculations.

The procedure that we followed for decomposition of the lines is described in Danezis et al. (2003). The way, criteria, and discussion about the model that we used to fit the observed spectral lines are presented in Danezis et al. (2003). They are explained in more detail in Lyratzi and Danezis (2004) and an application of the method is given in Popović et al. (2004). This means that we tried to fit the observed profiles of the Mg II resonance lines with fewer possible components. We at first tried to fit the observed spectral feature with one component. If this was not possible, we added one more component and then another, until we accomplished the best fit with fewer possible components. This means that we fitted the observed Mg II features with one to four components, for different stars. Our results are given in tables 2 and 3.

In order to be certain that we accomplished the best fit, we performed an F-test, between the fit that we accepted as being the best, and a fit with one component less. We present the results of the F-test in table 4, where we give the values of the confidence with which the accepted fit is better than the fit with one component less. We did not perform an F-test between the best fit and a fit with one component more, because this last one fit presented extreme differences with the observed spectral line profiles, or because the values of the measured parameters go against the classical theory for resonance lines (Danezis et al. 2003; Lyratzi & Danezis 2004).

4. Results and Discussion

The DAC phenomenon is quite common in O- and early B-type stars. However, we found that the DAC phenomenon is also observed in late B-type stars (as in the case of HD 144). Moreover, many researchers (Underhill 1975; Morgan et al. 1977; Marlborough et al. 1978; de Jager et al. 1979; Doazan 1982; Sahade et al. 1984; Sahade & Brandi 1985; Hutsemékers 1985), even if they did not use the name DACs, observed the same phenomenon. We also point out that in Underhill (1970), Marlborough, Snow, and Slettebak (1978), Dachs (1980), Doazan (1982), Sahade, Brandi, and Fontenla (1984), Sahade and Brandi (1985), Hutsemékers (1985), Doazan et al. (1991), and Cidale (1998) only the known DAC phenomenon was investigated. However, in the present paper a similar phenomenon of SACs is introduced, and we investigate whether this phenomenon is able to explain the complex structure of the Mg II resonance lines in the stellar spectra of all the Be spectral subtypes. Our result is that the SAC phenomenon is able to explain this complex structure.

Using the model described above, we find the best fit for the Mg II resonance lines of 64 Be stars given in table 1. In figure 3, we give the best fit of the Mg II resonance lines for two stars (HD 45910 and HD 41335). The first one (HD 45910) presents DACs, where the decomposition of the three different components is easy, while the second one (HD 41335) presents SACs, where it is hard to decompose the three different components without a convenient model. One can thus see that the model conveniently describes the Mg II complex profiles and the complex structure of the regions where these lines are created. In the studied IUE spectra, the interstellar lines are

Table 2. The kinematical parameters for absorption regions for considered stars.

Star	Spectral type	V_{rot1}	V_{rad1}	V_{rot2}	V_{rad2}	V_{rot3}	V_{rad3}	V_{rot4}	V_{rad4}
HD 5394	B0 IV evar	25	8.8	50	12.3				
HD 53367	B0 IV e	24	−18.0	37	−12.0	71	−7.0		
HD 203374	B0 IV pe	24	4.5	36	3.5	60	2.0		
HD 206773	B0 V pe	28	15.5	46	18.5				
HD 200310	B1 V e	25	10.1						
HD 212571	B1 V e	22	−2.5	40	−11.0				
HD 44458	B1 V pe	22	−17.5	37	−19.5	83	−29.0		
HD 200120	B1.5 V nne	28	−0.4						
HD 193237	B2 pe	30	−18.6	45	−18.1	86	(DAC) −200.6	115	(DAC) −200.1
HD 45910	B2 III e	24	13.0	42	11.0	60	(DAC) −229.5	170	(DAC) −182.0
HD 37202	B2 IV p	29	−18.0	48	−21.0			125	−33.0
HD 36576	B2 IV–V e	29	−43.0			80	−21.0		
HD 212076	B2 IV–V e	20	−1.0	34	−1.5				
HD 32991	B2 V e	19	−15.4	38	−21.9				
HD 58050	B2 V e	25	−35.9	49	−28.4				
HD 164284	B2 V e	28	13.3			63	33.8		
HD 41335	B2 V ne	22	−9.5	38	−1.5	80	27.0	100	40.0
HD 52721	B2 V ne	18	12.3	34	11.3	65	31.3		
HD 58343	B2 V ne	21	−1.8	50	−5.2				
HD 148184	B2 V ne	17	19.9	30	20.9				
HD 202904	B2 V e	20	4.0	31	4.5				
HD 65079	B2 V ne	29	8.0			74	−12.5		
HD 28497	B2 V ne	8	−45.0	37	−34.5	60	−35.0		
HD 45995	B2 V nne	29	−17.0	45	−20.0	69	−24.0		
HD 10516	B2 V pe	22	−1.0	37	−2.3	50	−5.8		
HD 187567	B2.5 IV e	19	23.6	32	24.6	50	26.1		
HD 32343	B2.5 V e	20	8.4			78	17.9		
HD 65875	B2.5 V e	17	14.0	35	18.0				
HD 191610	B2.5 V e	20	−45.6	45	−53.6				
HD 60855	B2/B3 V			45	−14.6	71	22.9	139	−29.6
HD 37490	B3 III e	20	−5.3	35	−8.3	54	−18.8	98	−10.3
HD 50820	B3 IV e+...	24	−13.0	50	−9.5				
HD 25940	B3 V e	22	0.7	42	−2.3				
HD 45725	B3 V e	18	−9.5	34	−10.5	65	−13.0		
HD 183362	B3 V e	24	24.2	34	24.2	68	19.7		
HD 208057	B3 V e	23	12.3			75	9.8		
HD 205637	B3 V p	22	17.5	39	15.5			115	9.0
HD 217543	B3 V pe	26	16.5	51	15.5			130	23.5
HD 217050	B4 III pe	35	14.3	54	17.8	84	32.3		
HD 89884	B5 III			33	−9.5	60	1.5		
HD 22192	B5 V e	16	−2.0	32	−1.0	52	−7.0		
HD 23302	B6 III e	21	−9.9			86	−8.9		
HD 45542	B6 III e	15	−24.4	33	−24.9	58	−15.4		
HD 109387	B6 III pe	18	−11.4			66	−28.4		
HD 23480	B6 IV e	20	−7.7	32	0.3				
HD 217891	B6 V e	18	−0.8						
HD 138749	B6 V nne	27	22.5	47	14.5				
HD 23630	B7 III	20	−9.0	45	−9.0				
HD 209409	B7 IV e	21	−9.0	38	−9.0	83	−5.0		

Table 2. (Continued.)

Star	Spectral type	$V_{\mathrm{rot}1}$	$V_{\mathrm{rad}1}$	$V_{\mathrm{rot}2}$	$V_{\mathrm{rad}2}$	$V_{\mathrm{rot}3}$	$V_{\mathrm{rad}3}$	$V_{\mathrm{rot}4}$	$V_{\mathrm{rad}4}$
HD 6811	B7 V e	19	3.3	35	1.8			169	12.8
HD 192044	B7 V e	25	19.5	52	8.5				
HD 210129	B7 V ne	21	62.6	52	43.1				
HD 142983	B8 Ia/Iab	21	−7.0	39	8.0	60	11.5	95	16.5
HD 29866	B8 IV ne	26	−42.0			85	41.5		
HD 47054	B8 V e	24	−30.0	42	−31.5				
HD 183914	B8 V e	17	16.8	37	20.8				
HD 50138	B8 V e	27	−36.0						
HD 58715	B8 V var	22	−21.5	44	−9.0				
HD 23552	B8 V ne			33	24.7				
HD 185037	B8 V ne	26	12.0	45	18.0				
HD 199218	B8 V nne	17	4.7	35	4.2			95	7.7
HD 91120	B8/B9 IV/V	23	−13.5	39	−15.0				
HD 142926	B9 pe	18	−12.9	50	2.1	67	7.6	165	3.6
HD 144	B9 III e	28	−30.6	53	(DAC) −188.6	80	(DAC) −187.1	178	(DAC) −129.6

The rotational (V_{rot}) and the radial (V_{rad}) velocities in km s^{-1}.

systematically shifted to the red for $+99\pm16$ km s^{-1}. We used the Hipparcos catalogues,[3] and we applied the corrections for the systemic velocity of individual stars (Smith 2001) and for the orbital motion of the those stars that are members of binary systems. Our results, given in tables 2 and 3 as well as in figures 4–8, are correspondingly corrected.

We should note that in our sample, 15 binary and multiple systems are present (see table 1). Considering that the origin of DACs and SACs might in principle be different than in single stars, at the beginning we separately analyzed this kind of star (presented with open circles in figures 4–6). However, we found that there is no systematic difference between single and binary/multiple stars. Consequently, in a further analysis we will not treat binary/multiple systems in a different way.

From the fit we obtained the rotational (V_{rot_i}) and radial (V_{rad_i}) velocities for each Mg II resonance line originating within the region.

In tables 2 and 3, we present the kinematical parameters for the absorption Mg II resonance line forming regions (table 2), as well as for the emission ones (table 3). As one can see, not all of the studied stars have an emission component, but only those listed in table 3. One could assume that these emission components are the emission part of P Cygni profiles formed by scattering. In that case, their wavelength and width do not represent the radial and rotational velocities. This could explain the majority of positive radial velocities since, in such a case as outflowing wind, lines will be widened and red-shifted. However, two cases with large negative radial velocities indicate that the real picture may be more complicated. We know that disk models, in many cases, may produce theoretically only the shape of the line profiles, but they are not able to fit them. Thus, in such cases, we may consider that the observed profile results from a different mechanism. In table 2, we give a list of stars, their spectral subtype (columns 1 and 2, respectively) and the values of the rotational velocities (columns 3, 5, 7, and 9) and the radial velocities (columns 4, 6, 8, and 10) of the respective

Table 3. The same as in table 2, but for the emission component where it is present.

Star	Spectral type	$V_{\mathrm{rot,e}}$	$V_{\mathrm{rad,e}}$
HD 203374	B0 IV pe	20	72
HD 45910	B2 III e	34	81
HD 32991	B2 V e	57	13
HD 164284	B2 V e	120	−1
HD 148184	B2 V ne	50	33
HD 45995	B2 V nne	46	102
HD 65875	B2.5 V e	30	53
HD 50820	B3 IV e+...	59	−87
HD 217891	B6 V e	50	6
HD 192044	B7 V e	94	7
HD 210129	B7 V ne	97	−29
HD 47054	B8 V e	81	0
HD 50138	B8 V e	53	120
HD 199218	B8 V nne	131	15

components. Also, in table 3, we present the kinematical parameters of the emission component. In column 1 we present a list of stars, in column 2 their spectral subtype and in columns 3 and 4 values of the rotational and radial velocities, respectively. Let us point out, here, that the calculated values correspond to the regions that create the SACs or DACs. Especially, the obtained rotational velocities correspond to the rotation of the region around itself and not around the star.

In figures 4 and 5, we present, separately, the rotational velocities and the radial velocities, respectively, of all the SACs as a function of the spectral subtype. In figure 5, the radial velocity's values that correspond to the DACs are clearly shown. In figure 6, we present the radial velocities of all the SACs as a function of the respective rotational velocities. In figure 7, we present mean values of the rotational and radial velocities of the two resonance lines of the emission component as a function of the spectral subtype. Each point

---

[3] ⟨http://vizier.u-strasbg.fr/viz-bin/VizieR-3⟩.

Table 4. Values of the confidence with which the accepted fit is better than the fit with the one less component.

Star	4–3 comps	3–2 comps	2–1 comps	Star	4–3 comps	3–2 comps	2–1 comps
HD 5394		0.9132		HD 25940		0.9972	
HD 53367	1.0000			HD 45725		1.0000	
HD 203374	0.9483			HD 183362	0.9807		
HD 206773		1.0000		HD 208057		1.0000	
HD 200310			0.9993	HD 205637	1.0000		
HD 212571		0.9826		HD 217543	1.0000		
HD 44458	0.9981			HD 217050	1.0000		
HD 200120			1.0000	HD 89884		1.0000	
HD 193237	1.0000			HD 22192		1.0000	
HD 45910	0.1609			HD 23302		1.0000	
HD 37202	1.0000			HD 45542		0.9998	
HD 36576		0.9931		HD 109387	0.9996		
HD 212076		1.0000		HD 23480		0.9998	
HD 32991		0.6737		HD 217891			
HD 58050		0.9978		HD 138749		0.9936	
HD 164284		0.7826		HD 23630		0.9986	
HD 41335	1.0000			HD 209409		0.9954	
HD 52721		0.9767		HD 6811	1.0000		
HD 58343		0.9928		HD 192044		0.8070	
HD 148184		0.9396		HD 210129		0.8927	
HD 202904		0.9475		HD 142983	1.0000		
HD 65079	1.0000			HD 29866		1.0000	
HD 28497	1.0000			HD 47054		0.9086	
HD 45995	0.1169			HD 183914		0.9975	
HD 10516	0.9981			HD 50138			0.6758
HD 187567		0.9747		HD 58715		0.9189	
HD 191610		0.9990		HD 23552			1.0000
HD 32343		0.7793		HD 185037		0.9500	
HD 65875		1.0000		HD 199218		0.9693	
HD 60855	0.9800			HD 91120		0.9778	
HD 37490	1.0000			HD 142926	1.0000		
HD 50820		0.6221		HD 144	1.0000		

refers to the mean value extracted for each spectral subtype. Finally, the radial velocities of the emission component as a function of the respective rotational velocities are shown in figure 8.

The values that we calculated lie within a small range, and we can obtain only the mean values of the radial and rotational velocities and their standard deviations. The points in the diagrams correspond to the mean values of the velocities for each spectral subtype, and the error bars that appear in some of the diagrams to the standard deviation. This standard deviation is not only a statistical error, but it also includes any possible variation of the inclination axis and the error of the spectral classification, since the spectral classification that was based in the optical range could not be appropriate for the UV range. This means that the error bars that appear in the diagrams include the statistical error as well as the dispersion of the values due to a different axis inclination.

The reproduction of the Mg II resonance lines $\lambda\lambda$ 2795.523, 2802.698 Å, using the model where SACs are present, suggests that the atmospherical regions where the Mg II doublet is created may be described in a unique way for all of the studied Be stars. This result confirms the suggestion given by de Jager et al. (1979) that in Be stellar atmospheres there exists a concentration of low-ionization species in the stellar wind, which is due to the occurrence of significant density variations. This result is also in agreement with the results of Morgan, Kondo, and Modisette (1977), who proposed that there are "significant absorption features" on the left side of each resonance line, which are attributed to "additional absorption within the stellar extended atmosphere". These "significant absorption features" can be the SACs that appear in the spectra of the early-type stars. Danezis et al. (2003) and Lyratzi and Danezis (2004) suggested that the peculiar phenomena observed in the spectra of Oe and Be stars, such as the SACs, are due to independent density regions in the stellar environment. Such regions may be structures that cover all, or a significant part, of the stellar disk (shells, blobs, puffs, and bubbles) (Underhill 1975; de Jager et al. 1979; Lamers et al. 1980; Henrichs 1984; Underhill & Fahey 1984; Bates & Halliwell 1986; Grady et al. 1987; Waldron et al. 1992; Cranmer & Owocki 1996; Kaper et al. 1996, 1997, 1999; Rivinius et al. 1997; Markova 2000), interaction
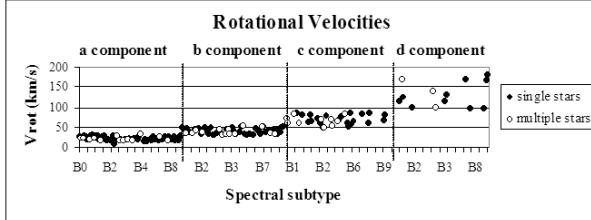
Fig. 4. Mean values for each spectral subtype of the rotational velocities of all the SACs as a function of the spectral subtype.
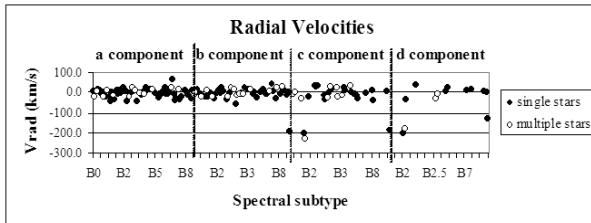
Fig. 5. Mean values for each spectral subtype of the radial velocities of all the SACs as a function of the spectral subtype.
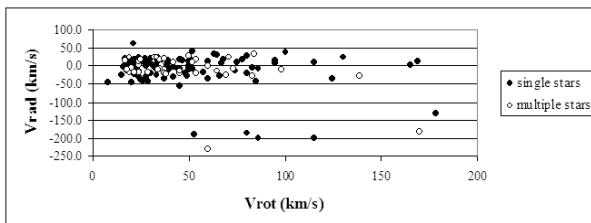
Fig. 6. Radial velocities of all the SACs as a function of the respective rotational velocities.

Fig. 7. Mean values for each spectral subtype of the rotational and radial velocities of the emission component as a function of the spectral subtype.

Fig. 8. Radial velocities of the emission component as a function of the respective rotational velocities.

regions of fast and slow wind components, CIRs, structures due to magnetic fields or spiral streams as a result of the stellar rotation (Underhill & Fahey 1984; Mullan 1984a, 1984b, 1986; Prinja & Howarth 1988; Cranmer & Owocki 1996; Kaper et al. 1996, 1997, 1999; Fullerton et al. 1997; Cranmer et al. 2000). This is the common theory that explains the DAC phenomenon in early-type stars. We found DAC phenomena in early B-type stars (e.g., HD 45910), as well as in late B-type stars (e.g., HD 144).

As one can see from table 2, the SAC phenomenon appears to be a classical one for the Be stars. In figure 3 and in table 2 one can see that all of the studied stars present discernible (DACs) or indiscernible (SACs) components of the Mg II resonance lines. The indiscernible components appear in the spectra of all of the stars of luminosity classes IV and V, and most of the stars of luminosity class III. It is very interesting that the SACs are observed as discrete lines (DACs) in the spectra of the three stars, HD 193237 (B2 pe), HD 45910 (B2 III e), and HD 144 (B9 III e), because they present quite different radial shifts. This means that the regions that
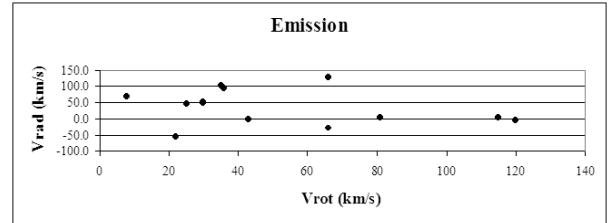
create these lines move radially with relatively large velocities, producing lines shifted enough to be easily observed in the spectra. On the other hand, in the case of all of the other studied stars, the SACs of the Mg II resonance lines present similar radial velocities, resulting in the SACs being blended among themselves. In this case, we can distinguish these lines by systematic differentiations of the rotational velocities.

The decomposition of the observed profiles for the Mg II regions in Be stellar atmospheres confirms the existence of independent density regions, since by using such a structure, we were able to reproduce the resonance lines of Mg II in all of the studied stars. This decomposition is physically meaningful, since it enables us to detect kinematically different regions with different rotational and radial velocities, as well as the optical depth and the column density, for each of the Mg II independent density regions, which produce DACs or SACs.

Our analysis shows that regions where the considered Mg II resonance lines originate ("blobs" and "puffs" created by winds or cool extended envelopes) may consist of more independent density layers of matter with different kinematical properties (one to four in the analyzed cases). We identified them by the decomposition of observed Mg II lines in the number of components that best fit the observed profile. Namely, depending on particular stars, we obtained that SACs or DACs may be divided in several rotational velocity groups (average values for rotational velocity groups found to be present at 64 considered stars are 22 ± 5 km s^{-1}, 41 ± 7 km s^{-1}, 69 ± 11 km s^{-1}, and 130 ± 31 km s^{-1}). The corresponding radial velocities are near zero (-3.3 ± 20.3 km s^{-1} for the first density region, -3.6 ± 20.6 km s^{-1} for the second one, -1.0 ± 21.8 km s^{-1} for the third one, and $+4.0\pm22.7$ km s^{-1} for the fourth one). In the spectra of the stars HD 193237 (B2 pe), HD 45910 (B2 III e), and HD 144 (B9 III e) the SACs appear as discrete components (DACs), and the radial velocities of the

third and the fourth density regions are -205.7 ± 21.7 km s^{-1} and -170.6 ± 36.6 km s^{-1}, respectively. In the case of the star HD 144, the second component also appears as a discrete component. The radial velocity of the region that creates this component is -188.6 km s^{-1} (figures 4, 5, and 6). The observed velocity dispersion may be due to the different values of the rotational axis inclination of the regions where the SACs are created. The results presented above confirm that the Mg II doublet is more or less stable for a given spectral type as Gurzadyan (1975) suggested. We did not find any variation of the velocities in the Mg II regions with the luminosity class, except in the case of the peculiar stellar spectra, where the SACs appear as discrete lines (DACs), while Kondo, Morgan, and Modisette (1976) proposed that, apart from the difference among spectral subtypes, there is probably difference among luminosity classes too.

We assume that independent density regions corresponding to particular components of considered Mg II lines (one to four components corresponding to one to four regions in the case of 64 stars analyzed here) lie all in the cool stellar envelope. Depending on the temperature, different ions with different ionization potential are created in different regions at different distances from the star. This means that the spectral lines observed in the spectra of Be stars are derived from specific atmospherical regions, different among themselves. The ions that are created very close to the star lie in regions that present spherical symmetry around the star (case A in figure 1). On the other hand, the ions that are created at long distance from a star lie in regions that present spherical symmetry around their own center, and not around the star (case B in figure 1). As the ionization potential of the Mg II ions is I.P.=7.646 eV, the Mg II ions can be created only at great distance from the center of the star, i.e., in the disk, where spherical symmetry around the star cannot be accepted. This means that the Mg II ions lie at regions which present topical or apparent spherical symmetry (case B in figure 1). As a result, the Mg II spectral lines and their SACs/DACs may be derived only from such regions (case B in figure 1), and not from classically spherical regions around the star (case A in figure 1). This kind of density regions (blobs) has been proposed by many researchers (Underhill 1975; de Jager et al. 1979; Lamers et al. 1980; Henrichs 1984; Underhill & Fahey 1984; Mullan 1984a, 1984b, 1986; Bates & Halliwell 1986; Grady et al. 1987; Prinja & Howarth 1988; Waldron et al. 1992; Cranmer & Owocki 1996; Kaper et al. 1996, 1997, 1999; Fullerton et al. 1997; Rivinius et al. 1997; Markova 2000; Cranmer et al. 2000) and are detected in many other cases, as in active stars (WR 104, see figure 2) and many quasars, as we observe DACs/SACs in their UV spectra (Danezis et al. 2006). This means that the density regions are a common phenomenon, observed at different levels. The fact that we found one to four components is accidental. In principle, there could be more or less. Although the number of components is different in different stars, we may conclude that the Mg II resonance lines forming regions present a complex structure.

Our proposition that the SAC phenomenon is responsible for the structure of Mg II lines means that we theoretically expect that the Mg II components have similar radial velocities, within the range of the statistical error (~ 10 km s^{-1}). The problem

was how to distinguish them. The common idea (Doazan 1982) is that the radial velocity of the kinematically independent regions is a function of the distance from the rapidly rotating Be star. Accordingly, our first thought was to distinguish these regions according to their rotational velocities, which was confirmed by our calculations. Namely, the regions that create the Mg II lines have similar radial velocities and different rotational velocities.

In our sample we could not detect high radial velocities, no matter what method we used (the proposed model or any other classical method). The radial velocities of all the SACs, in all the studied stars, are about 0 km s^{-1}, and only in the case of the stars HD 193237 (B2 pe), HD 45910 (B2 III e), and HD 144 (B9 III e), where we observed DACs, did we calculate radial velocities with values between -130 km s^{-1} and -230 km s^{-1}. We could detect the same phenomenon in the case of Si IV in a sample of 68 Be stars (values of radial velocities between -116 km s^{-1} and $+25$ km s^{-1}) (Lyratzi et al. 2006), as well as in the case of Hα in 120 Be stars (values of radial velocities around 0 km s^{-1}) (Lyratzi et al. 2005). These results indicate that in the atmospherical layers from the photosphere (very broad components of Hα) to the cool envelope (Mg II resonance lines) we cannot detect very high radial velocities. However, as we expected, the presence of DACs in three stars of our sample indicated that from the regions near to the star toward the ones away from the star, the radial velocity increases, but it does not reach high values, as happens in the case of Oe stars. In the case of specific Be stars that present the DACs with high radial velocities in some of their spectra, e.g., 59 Cyg and γ Cas (Doazan et al. 1989; Telting & Kaper 1994), we should study each one of them as an exception of the classical rule. This proposition is based on the fact that the spectral classification was made in the optical range, and may not apply in the UV spectral range (Walborn 1971; Walborn & Panek 1984; Walborn & Nichols-Bohlin 1987) (see also the SIMBAD database[4]). This means that the spectral classifications in the optical and the UV ranges are not always in accord. As a result, some early Be stars could be late Oe stars, and we know that it is a common phenomenon to observe high radial velocities of SACs/DACs in Oe stars. However, in the case of Be stars, we have not observed the same phenomenon. This difference in the behavior of density regions in Oe and Be stars is very interesting and requires further investigation. Finally, we should pay attention to the way that the radial velocities are calculated. The classical method considered that the whole observed feature corresponds to only one spectral line, meaning that the radial velocity was calculated by the displacement of the deeper point of the observed feature. Considering the SAC idea, the observed feature consists of a number of spectral line components. As a result, the deeper point of the observed feature is only the result of the synthesis of all the SACs. In this case we should calculate the radial velocity of every one of these components.

An emission component is present in the spectra of B0, B2, B2.5, B3, B6, B7, B8, and B9 type stars (figure 7). This means that emission does not appear in the spectra of the middle spectral subtypes of Be stars (Kondo et al. 1975). The radial

---

[4] ⟨http://simbad.u-strasbg.fr/sim-fid.pl⟩.
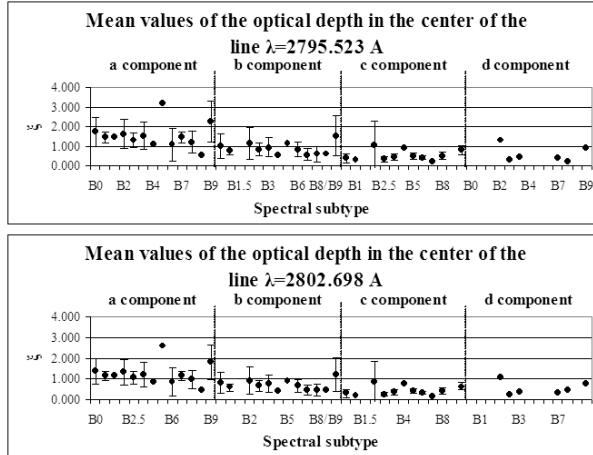
Fig. 9. Mean values of the optical depth, ξ, in the center of the line for all kinematically separated components of each resonance line, as a function of the spectral subtype.

velocity of the emission component decreases as the rotational velocity increases. The emission component presents positive or negative radial velocity. If one takes into account that negative radial velocities exist, which is not in agreement with the assumption that all emission components are the emission part of P Cygni profiles formed by scattering, one can assume the following. The obtained velocities correspond to the regions where the emission component is created as, e.g., strings, blobs, puffs, bubbles. This means that the emission region may approach, or move away from, the observer, and its different position and motion around the star is responsible for whether this value is positive or negative. In figures 7 and 8, one can see that as the rotational velocity increases the radial velocity decreases, in contrast to the relation of the two velocities of the absorption components. A problem with the emission component is that it is blended with the absorption lines of other ions, and thus it is difficult to evaluate the rotational and radial velocities. As a result, the calculated values present greater statistical error than in the case of the absorption components.

According to the criteria described in Danezis et al. (2003), the same components of the two resonance lines should have the same values of rotational and radial velocities and the ratio of the optical depth (ξ) should be the same as the respective ratio of the relative intensities. In figure 9, we present the mean values of the optical depth (ξ) in the center of the line for all kinematically separated components of each resonance line, as a function of the spectral subtype. As one can see, the value of ξ of the first kinematical region is obviously higher than in the other three. It tends to decrease from the first kinematical region to the fourth. That, also, may indicate physically separated regions.

5. Conclusions

We applied a method developed in Danezis et al. (2003) and Lyratzi and Danezis (2004) to the Mg II resonance line of 64 Be stars in order to investigate the kinematical properties of the Mg II resonance line forming region. We obtained the rotational and radial velocities, which allowed us to extract some general physical properties concerning the Mg II regions of Be stars. Some interesting results inferred from the investigations are the following: (i) The proposed rotation model gives satisfactory results for the region of the Mg II $\lambda\lambda$ 2795.523, 2802.698 Å resonance lines. (ii) The atmospherical absorption region where the Mg II resonance lines are created presents a complex structure. It tends to be composed by more than one kinematically independent region (only four stars present a simple structure). We found that the kinematically independent regions rotate with different velocities: 22 km s^{-1}, 41 km s^{-1}, 69 km s^{-1}, and 130 km s^{-1}. The respective radial velocities are near to zero for all of these regions. These calculated values lead us to accept that the Mg II resonance lines of the Be stellar spectra present Satellite Absorption Components (SACs). (iii) The rotational velocities of the found independent regions present a uniform fluctuation with the spectral subtype. (iv) The emission lines were detected for the earliest and latest spectral subtypes with positive radial velocities with several exceptions; i.e., they have negative radial velocities ranging from 0 to -87 km s^{-1}. If lines are formed by scattering, the positive values are not radial velocities.

Appendix.   Calculation of the Distribution Function L

As we know, the distribution function (L) of the absorption coefficient (k_λ) has the same form as the distribution function of each component of the spectral line. This means that we can replace the distribution function of the absorption coefficient, L_i, with another expression for the distribution function of each component.

It is also known that Be and Oe stars are rapid rotators. This means that we accept that the main reason for the line broadening is rotation of the regions that produce each satellite component of the whole observed spectral feature. These rapidly rotating density regions may also present radial motion. For these two reasons, we seek another expression for the distribution function of the spectral line's components that has as parameters the rotational and radial velocities of the spherical density regions.

For a spherical density region, we assume the following hypotheses: i) the natural broadening of the spectral lines follows the Lorentz distribution; ii) Lambert's sinus law stands for each point of the spherical region; iii) the angular velocity of rotation is constant.

In order to calculate the total radiation, we divide the
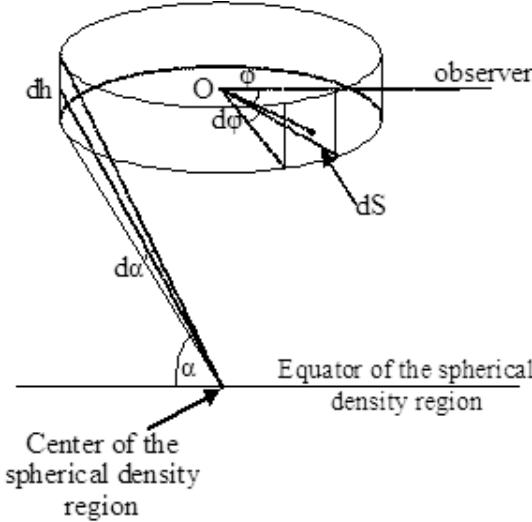
Fig. 10. Elementary ring of the spherical density region.

spherical layer in very thin cylindrical surfaces that are perpendicular to the rotational axis. Lambert's law allows us to consider that the luminosity from each point on the sphere is the same.

On the above cylindrical surface we also consider the surface dS. According to Lambert's law, when this surface rotates with an angular velocity ω, its radiation intensity is

$$dI(\omega) = Q(\omega)dS\cos\theta, \tag{A1}$$

where θ is the angle between the vertical on dS and the line of sight and

$$Q(\omega) = C_1 \frac{\gamma}{(\omega - \omega_k)^2 + \left(\frac{\gamma}{2}\right)^2}. \tag{A2}$$

C_1 is a constant and γ is the Lorentzian full width at half maximum, which in the case of natural broadening has a value of $\gamma \cong 10^8$ Hz.

When the surface dS does not rotate, the center of the formed spectral line has the observed wavelength, λ_0, which corresponds to a frequency, ν_0. Thus,

$$\omega_0 = 2\pi\nu_0 = 2\pi\frac{c}{\lambda_0}. \tag{A3}$$

When the surface dS rotates with a rotational velocity $V_{\rm rot}$, the center of the formed line has the wavelength λ_k, and in this case $\omega_k = \omega_0(1 - z\sin\varphi)$, where $z = V_{\rm rot}/c$.

We also have $\cos\theta \cong \cos\alpha\cos\varphi$. The angles α and φ are shown in figure 10.

The surface dS can be written as $dS = rdhd\varphi$, where r is the radius of the cylinder, $d\varphi$ the angle under which the observer sees dS, and dh the height of dS.

Making the above substitutions in equation (A1), we have

$$dI(\omega) = \frac{C_1 rdh\gamma\cos\alpha\cos\varphi d\varphi}{[\omega - \omega_0(1 - z\sin\varphi)]^2 + \left(\frac{\gamma}{2}\right)^2}. \tag{A4}$$

Thus, the radiation intensity from the semicylinder is

$$I(\omega) = \int_{-\pi/2}^{\pi/2} \frac{C_1 rdh\gamma\cos\alpha\cos\varphi d\varphi}{[\omega - \omega_0(1 - z\sin\varphi)]^2 + \left(\frac{\gamma}{2}\right)^2} \tag{A5}$$

or

$$I(\omega) = \frac{4C_1 rdh}{\gamma}$$
$$\times \int_{-\pi/2}^{\pi/2} \frac{\cos\alpha d(\sin\varphi)}{\{[\omega/(\gamma/2)] - [\omega_0/(\gamma/2)](1 - z\sin\varphi)\}^2 + 1}. \tag{A6}$$

If we take that $\tilde\omega = \omega/(\gamma/2)$, $\tilde\omega_0 = \omega_0/(\gamma/2)$, $x = \sin\varphi$, we have

$$I(\tilde\omega) = \frac{4C_1 r\cos\alpha dh}{\gamma}\int_{-1}^{1} \frac{dx}{[\tilde\omega - \tilde\omega_0(1 - zx)]^2 + 1}. \tag{A7}$$

Taking that $y = \tilde\omega - \tilde\omega_0(1 - zx)$, the above integral becomes

$$I(\tilde\omega) = \frac{4C_1 r\cos\alpha dh}{\gamma\tilde\omega_0 z}\int_{\tilde\omega - \tilde\omega_0(1+z)}^{\tilde\omega - \tilde\omega_0(1-z)} \frac{dy}{y^2 + 1}. \tag{A8}$$

Finally, we have

$$I(\tilde\omega) = \left(\frac{4C_1 r\cos\alpha dh}{\gamma}\right)$$
$$\times \left(\frac{\arctan[\tilde\omega - \tilde\omega_0(1-z)] - \arctan[\tilde\omega - \tilde\omega_0(1+z)]}{\tilde\omega_0 z}\right). \tag{A9}$$

The above function describes the radiation intensity from a visual semicylinder with radius r and height dh.

Under the angle $d\alpha$ is seen dh from the center of the spherical region. This cylinder rotates with a rotational velocity, $z = V_{\rm rot}/c$, and a constant angular velocity, $\tilde\omega$.

We consider the function

$$P(\tilde\omega, z) = \frac{\arctan[\tilde\omega - \tilde\omega_0(1-z)] - \arctan[\tilde\omega - \tilde\omega_0(1+z)]}{\tilde\omega_0 z}. \tag{A10}$$

We study the limit of this function in the case that the density layer does not rotate, i.e., when $z \to 0$. In such a case,

$$\lim_{z\to 0} P(\tilde\omega, z)$$
$$= \lim_{z\to 0} \frac{\arctan[\tilde\omega - \tilde\omega_0(1-z)] - \arctan[\tilde\omega - \tilde\omega_0(1+z)]}{\tilde\omega_0 z}. \tag{A11}$$

We apply L' Hospital's theorem and we obtain

$$\lim_{z\to 0} P(\tilde\omega, z)$$
$$= \lim_{z\to 0} \frac{\frac{d}{dz}\{\arctan[\tilde\omega - \tilde\omega_0(1-z)]\} - \frac{d}{dz}\{\arctan[\tilde\omega - \tilde\omega_0(1+z)]\}}{\frac{d}{dz}(\tilde\omega_0 z)}, \tag{A12}$$
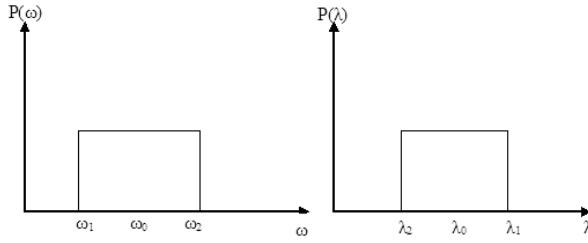
Fig. 11. Quadratic pulsation.
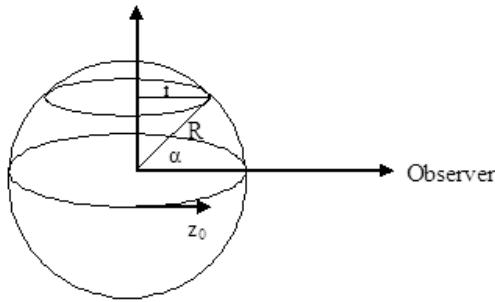
Fig. 12. Rotating spherical density region that produces SACs or DACs.

$$\lim_{z \to 0} P(\tilde{\omega}, z)$$

$$= \lim_{z \to 0} \left[\frac{1}{1 + [\tilde{\omega} - \tilde{\omega}_0(1 - z)]^2} + \frac{1}{1 + [\tilde{\omega} - \tilde{\omega}_0(1 + z)]^2} \right]$$

$$= \frac{2}{(\tilde{\omega} - \tilde{\omega}_0)^2 + 1}. \tag{A13}$$

It is obvious that in the nonrotating case this form corresponds to the Lorentz's distribution for the naturally broadened spectral lines.

In the case where the rotation broadening, $|\lambda_1 - \lambda_2|$ (or $|\omega_1 - \omega_2|$), is much larger than the natural broadening (the natural broadening of a spectral line is of an order of 10^{-3}–10^{-4}Å), the above function, $P(\tilde{\omega}, z)$, presents the form of one quadratic pulsation (see figure 11)

For each ω with $\omega_1 < \omega < \omega_2$, the relative shift is $z = |\Delta\omega|/\omega_0$. For a point ω_1 we have $(\omega_0 - \omega_1)/\omega_0 = z$, so that $\omega_1 = \omega_0(1 - z)$. Likewise, for a point ω_2 we have $\omega_2 = \omega_0(1 + z)$. But, $\omega = 2\pi\nu = 2\pi c/\lambda$. Thus, $\lambda_1 = \lambda_0/(1 - z)$ and $\lambda_2 = \lambda_0/(1 + z)$ with $\lambda_1 > \lambda_2$.

This means that $\Delta\lambda_{\rm total} \equiv \lambda_1 - \lambda_2 = 2\lambda_0 z/(1 - z^2)$ and so $\lambda_{\min} \equiv \lambda_2 = \lambda_0 - \Delta\lambda_{\rm total}/2 = \lambda_0 - \lambda_0 z/(1 - z^2)$ and $\lambda_{\max} \equiv \lambda_1 = \lambda_0 + \Delta\lambda_{\rm total}/2 = \lambda_0 + \lambda_0 z/(1 - z^2)$.

We set $\rho = \lambda_0 z/(1 - z^2)$ and normalize to 1. In this way, the function $P(\tilde{\omega}, z)$ could be approximated by the function $f(\lambda)$ where:

$$f(\lambda) = \begin{cases} 1 & |\lambda - \lambda_0| < \rho \\ 0 & \text{otherwise} \end{cases}. \tag{A14}$$

We now assume that the spherical density region rotates with equatorial velocity $z_0 = V_0/c$ (figure 12).

The points of the circle with radius r rotate with a velocity $V_{\rm rot}$ and for $r = R\cos\alpha$ we take $V_{\rm rot} = \omega r = \omega R\cos\alpha$.

We set $V_0 = \omega R$. Also, $\omega = $ const. Thus, $V_{\rm rot} = (V_0/R)R\cos\alpha = V_0\cos\alpha$ and $z = z_0\cos\alpha$. We also have $dh = Rd\alpha$ and equation (A1) becomes

$$dI(\tilde{\omega}) = \frac{4C_1 R}{\gamma}$$

$$\times \frac{\arctan[\tilde{\omega} - \tilde{\omega}_0(1 - z_0\cos\alpha)] - \arctan[\tilde{\omega} - \tilde{\omega}_0(1 + z_0\cos\alpha)]}{\tilde{\omega}_0 z_0 \cos\alpha}$$

$$\times \cos\alpha d\alpha. \tag{A15}$$

The integral of this equation is

$$I(\tilde{\omega}) = \frac{4C_1 R}{\gamma}$$

$$\times \int_{-\pi/2}^{\pi/2} \frac{\arctan[\tilde{\omega} - \tilde{\omega}_0(1 - z_0\cos\alpha)] - \arctan[\tilde{\omega} - \tilde{\omega}_0(1 + z_0\cos\alpha)]}{\tilde{\omega}_0 z_0 \cos\alpha}$$

$$\times \cos\alpha d\alpha. \tag{A16}$$

When we take into account the function $P(\tilde{\omega}, z)$, the above function becomes

$$I(\tilde{\omega}) = \frac{4C_1 R}{\gamma} \int_{-\pi/2}^{\pi/2} P(\tilde{\omega}, z_0\cos\alpha)\cos\alpha d\alpha. \tag{A17}$$

We approximate $P(\tilde{\omega}, z_0\cos\alpha)$ at $f(\lambda)$ and take the integral for the observation angle $\theta \in [-\theta_0, \theta_0]$ from the equatorial plane.

We have

$$I(\tilde{\omega}) \cong I_1 = \frac{4C_1 R}{\gamma} \int_{-\theta_0}^{\theta_0} 1 \cdot \cos\theta d\theta, \tag{A18}$$

$$I_1 = \frac{4C_1 R}{\gamma} \int_{-\theta_0}^{\theta_0} \cos\theta d\theta = \frac{4C_1 R}{\gamma}[\sin\theta]_{-\theta_0}^{\theta_0} = \frac{8C_1 R}{\gamma}\sin\theta_0. \tag{A19}$$

If we normalize the constant, we have

$$I_1 = \sin\theta_0 = \sqrt{1 - \cos^2\theta_0}. \tag{A20}$$

For angle θ_0 we have

$$|\lambda - \lambda_0| \le \rho_0 = \frac{\lambda_0 z_0 \cos\theta_0}{1 - z_0^2\cos^2\theta_0}. \tag{A21}$$

For a wavelength λ or for a shift of $\Delta\lambda = |\lambda - \lambda_0|$ from the center of the spectral line, the absorbing (or emitting) regions are those with angular distance θ from the equatorial plane, with $|\theta| \le \theta_0$.

For the equatorial plane we have

$$\Delta\lambda = \frac{\lambda_0 z_0 \cos\theta_0}{1 - z_0^2\cos^2\theta_0}. \tag{A22}$$

From this equation we can calculate the angle θ_0 as

$$\cos\theta_0 = \frac{-\lambda_0 \pm \sqrt{\lambda_0^2 + 4\Delta\lambda^2}}{2\Delta\lambda z_0}. \tag{A23}$$

Since θ_0 is between $-\pi/2$ and $\pi/2$, we have $\cos\theta_0 \geq 0$, and so

$$\cos\theta_0 = \frac{-\lambda_0 + \sqrt{\lambda_0^2 + 4\Delta\lambda^2}}{2\Delta\lambda z_0}. \tag{A24}$$

Thus, the distribution function I_1 takes its final form:

$$I_1 = \sqrt{1 - \cos^2\theta_0} \quad \text{if} \quad \cos\theta_0 = \frac{-\lambda_0 + \sqrt{\lambda_0^2 + 4\Delta\lambda^2}}{2\Delta\lambda z_0} < 1 \tag{A25}$$

and

$$I_1 = 0 \quad \text{otherwise.} \tag{A26}$$

It is obvious that the distribution function I_1 is a function of the wavelength (λ). This means that $I_1 = I_1(\lambda)$. This distribution function has the same form as the distribution function of the absorption coefficient, L, and may replace it (in $e^{-L\xi}$), when the main reason of the line broadening is rotation. We name it the rotation distribution function.

The spectral line profile, which is formed by a spherical density region, is reproduced by the function $e^{-L\xi}$ by applying an appropriate value of the rotational velocity, V_{rot} (from z_0), the radial velocity, V_{rad} [from $V_{\text{rad}}/c = (\lambda_0 - \lambda_{\text{lab}})/\lambda_{\text{lab}}$], and the optical depth, ξ, in the center of the line.

References

Bates, B., & Halliwell, D. R. 1986, MNRAS, 223, 673

Cidale, L. S. 1998, ApJ, 502, 824

Cowley, A. 1972, AJ, 77, 750

Cowley, A., Cowley, C., Jaschek, M., & Jaschek, C. 1969, AJ, 74, 375

Cranmer, S. R., & Owocki, S. P. 1996, ApJ, 462, 469

Cranmer, S. R., Smith, M. A., & Robinson, R. D. 2000, ApJ, 537, 433

Dachs, J. 1980, Second European IUE Conf. (ESA SP-157), (Paris: ESA), 139

Danezis, E. 1983, PhD Thesis, University of Athens

Danezis, E. 1987, in Physics of Be Stars, ed. A. Slettebak & T. P. Snow (Cambridge: Cambridge University Press), 445

Danezis, E., et al. 2003, Ap&SS, 284, 1119

Danezis, E., Popović, L. Č., Lyratzi, E., & Dimitrijević, M. S. 2006, in The Physics of Ionized Gases, ed. L. Hadzievski, B. Marinkovic, & N. Simonovic (AIP), 373

Danezis, E., Theodossiou, E., & Laskarides, P. G. 1991, Ap&SS, 179, 111

de Jager, C., Kondo, Y., Hoekstra, R., van der Hucht, K. A., Kamperman, T. M., Lamers, H. J. G. L. M., Modisette, J. L., & Morgan, T. H. 1979, ApJ, 230, 534

Doazan, V. 1982, in B Stars With and Without Emission Lines, ed. A. Underhill & V. Doazan (Washington, D. C. : NASA), 279

Doazan, V., Barylak, M., Rusconi, L., Sedmak, G., Thomas, R. N., & Bourdonneau, B. 1989, A&A, 210, 249

Doazan, V., Sedmak, G., Barylak, M., & Rusconi, L. 1991, A Be Star Atlas of Far UV and Optical High-Resolution Spectra (ESA SP-1147), (Noordwijk: ESA Publications Division)

Doazan, V., & Thomas, R. N. 1982, in B Stars With and Without Emission Lines, ed. A. Underhill & V. Doazan (Washington, D. C. : NASA), 409

Fullerton, A. W., Massa, D. L., Prinja, R. K., Owocki, S. P., & Cranmer, S. R. 1997, A&A, 327, 699

Grady, C. A., Sonneborn, G., Wu, C.-C., & Henrichs, H. F. 1987, ApJS, 65, 673

Guetter, H. H. 1968, PASP, 80, 197

Gurzadyan, G. A. 1975, PASP, 87, 289

Henrichs, H. F. 1984, Fourth European IUE Conf. (ESA SP-218), (Noordwijk: ESA), 43

Herbig, G. H., & Spalding, J. F., Jr. 1955, ApJ, 121, 118

Houk, N., & Smith-Moore, M. 1988, Michigan Catalogue of Two-Dimensional Spectral Types for HD Stars, vol.4

Houziaux, L., & Andrillat, Y. 1976, IAU Symp., 70, 87

Hutsemékers, D. 1985, A&AS, 60, 373

Kaper, L., et al. 1997, A&A, 327, 281

Kaper, L., Henrichs, H. F., Nichols, J. S., Snoek L. C., Volten, H., & Zwarthoed G. A. A. 1996, A&AS, 116, 257

Kaper, L., Henrichs, H. F., Nichols, J. S., & Telting, J. H. 1999, A&A, 344, 231

Kelly, R. L. 1979, Atomic Emission Lines in the Near Ultraviolet (NASA TM 80268), (Washington, D. C. : NASA)

Kondo, Y., Modisette, J. L., & Wolf, G. W. 1975, ApJ, 199, 110

Kondo, Y., Morgan, T. H., & Modisette, J. L. 1976, ApJ, 209, 489

Lamers, H. J. G. L. M., Faraggiana, R., & Burger, M. 1980, A&A, 82, 48

Laskarides, P. G., Theodossiou, E., & Danezis, E. 1992, Ap&SS, 179, 13

Lesh, J. R. 1968, ApJS, 17, 371

Lyratzi, E., & Danezis, E. 2004, AIP Conf. Proc., 740, 458

Lyratzi, E., Danezis, E., Antoniou, A., Nikolaidis, D., Popović, L. Č., & Dimitrijević, M. S. 2006, IAU Joint Discussion 4

Lyratzi, E., Danezis, E., Nikolaidis, D., Popović, L. Č., Dimitriević, M. S., Theodossiou, E., & Antoniou, A. 2005, Mem. Soc. Astron. Ital. Suppl., 7, 114

Lyratzi, E., Danezis, E., Stathopoulou, M., Theodossiou, E., Nikolaidis, D., Drakopoulos, C., & Soulikias, A. 2003, Publ. Astron. Obs. Belgrade, 76, 27

Markova, N. 2000, A&AS, 144, 391

Marlborough, J. M., Snow, T. P., Jr., & Slettebak, A. 1978, ApJ, 224, 157

Moore, C. E. 1968, National Bureau of Standard Circ., 488

Morgan, T. H., Kondo, Y., & Modisette, J. L. 1977, ApJ, 216, 457

Morgan, W. W., Code, A. D., & Whitford, A. E. 1955, ApJS, 2, 41

Mullan, D. J. 1984a, ApJ, 283, 303

Mullan, D. J. 1984b, ApJ, 284, 769

Mullan, D. J. 1986, A&A, 165, 157

Osawa, K. 1959, ApJ, 130, 159

Peton, A. 1974, Space Sci. Rev., 30, 481

Popović, L. Č., et al. 2004, AIP Conf. Proc., 740, 497

Prinja, R. K., & Howarth, I. D. 1988, MNRAS, 233, 123

Rivinius, T., et al. 1997, A&A, 318, 819

Sahade, J., & Brandi, E. 1985, Rev. Mex. Astron. Astrofis., 10, 229

Sahade, J., Brandi, E., & Fontenla, J. M. 1984, A&AS, 56, 17

Slettebak, A. 1954, ApJ, 119, 146

Slettebak, A., & Snow, T. P., Jr. 1978, ApJ, 224, L127

Smith, M. A. 2001, PASP, 113, 882

Telting, J. H., & Kaper, L. 1994, A&A, 284, 515

Tuthill, P. G., Monnier, J. D., & Danchi, W. C. 1999, Nature, 398, 487

Underhill, A. B. 1970, in Spectrum Formation in Stars With Steady-State Extended Atmospheres, ed. H. G. Groth & P. Wellman (Washington, D. C. : National Bureau of Standards), 3

Underhill, A. B. 1975, ApJ, 199, 691

Underhill, A. B., & Fahey, R. P. 1984, ApJ, 280, 712

Walborn, N. R. 1971, ApJS, 23, 257

Walborn, N. R., & Nichols-Bohlin, J. 1987, PASP, 99, 40

Walborn, N. R., & Panek, R. J. 1984, ApJ, 280, L27

Waldron, W. L., Klein, L., & Altner, B. 1992, ASP Conf. Ser., 22, 181